Unsteady Particle Deposition in a Human Nasal Cavity during Inhalation

Camby M.K. Se[1,2], Kiao Inthavong[1] and Jiyuan Tu[1]
[1]School of Aerospace, Mechanical and Manufacturing Engineering, RMIT University, PO Box 71, Plenty Road, Bundoora, Victoria 3083, Australia
[2]Department of Building and Construction, City University of Hong Kong, Tat Chee Avenue, Kowloon, Hong Kong SAR
E-mail: kiao inthavong@rmit.edu.au

Received: 15 March 2010, Accepted: 9 July 2010

Abstract
The present study investigates the deposition efficiency during the unsteady inhalation cycle by using Computational Fluid Dynamics (CFD). The unsteady inhalation profile was applied at the outlet of nasopharynx, which had a maximum flow rate of 40.3L/min which corresponds to an equivalent steady inhalation tidal volume flow rate of 24.6L/min. Aerodynamic particle sizes of 5μm and 20μm were studied in order to reflect contrasting Stokes numbered particle behaviour. Two particle deposition efficiencies in the nasal cavity versus time are presented. In general, the deposition of 5μm particles was much less than 20μm particles. The first 0.2 second of the inhalation cycle was found to be significant to the particle transport, since the majority of particles were deposited during this period (i.e. its residence time). Comparisons were also made with its equivalent steady inhalation flow rate which found that the unsteady inhalation produced lower deposition efficiency for both particle sizes.

1. INTRODUCTION

Respiratory-related disease is a critical health issue in metropolis cities due to huge emissions of irritating particulates from vehicles and unwanted products during industrial and manufacturing processes. Generally, large particles are less harmful than small particles because of their shorter residence time in the air. It has been shown that particles with an aerodynamic diameter of 80μm can achieve 50-80% aspiration efficiency through the mouth [1-3]. For nasal inhalation 80μm aerodynamic diameter particles achieve approximately 30% aspiration efficiency. For both types of inhalation, decreasing aerodynamic diameters produce an increase in the aspiration efficiency. This is significant as a large number of dusts and general pollutants are commonly found in the range of 1-80μm. Respiratory diseases such as influenza, and tuberculosis (TB), may result from excessive exposure of harmful respiratory bacteria. In severe cases deep lung deposition can occur, leading to loss of lung compliance and even lung cancer.

Experimental and numerical studies [1, 3] have shown that facial features, such as the nose, lips, cheeks etc., are able to reduce the inhalability of airborne particles. For those inhaled particles, the nasal cavity becomes another natural defence where a portion of particles will deposit before being removed by mucociliary action. Deposition of particles in the bronchus or the alveoli which are deep in the lungs should be avoided as the particles will accumulate, causing adverse health effects. In light of this, many experimental and numerical studies [4-7] of particle deposition in the nasal cavity have been performed to study the deposition and the probability of deep particle deposition in the lung.

During breathing, the inhalation and exhalation cycle flow rate varies with time. Particle deposition efficiency is known to have a strong correlation with the particle size and the airflow rate (e.g. diffusion parameter, $d_p^{1/2} / Q^{1/8}$ and inertial parameter, $d_p^2 Q$) where d_p is the aerodynamic diameter and Q is the flow rate. Both factors have been studied experimentally and numerically [8-10] resulting in two general findings: 1) deposition efficiency increases with the particle size; 2) deposition efficiency decreases with increases in the inhalation flow rate. In these studies, along with others in the literature [8, 11-12], a constant inhalation flow rate with a constant inlet velocity

at nostril surfaces was adopted. An in-vivo experimental study conducted by [13] highlighted that this approach neglects the acceleration during inhalation and thus leads to an overprediction in the particle deposition in comparison to a cyclic breathing pattern (i.e. unsteady inhalation). In their work, only the total deposition in a replicate of a nasal cavity was analysed versus inhalation flow rate, the time-dependent deposition characteristic along the nasal cavity was not discussed. In addition, earlier numerical studies [9, 14] used a steady flow field, determined at the nostril inlet by enforcing a velocity or mass flow rate boundary condition. Where both cavities of the nose was used an equivalent flow rate at each nostril gives the presumption of an equivalent flow distribution through each cavity, before the flow merges at the naospharynx, which is not necessarily correct. During the respiration cycle, the airflow through the nasal passage is normally asymmetrical where one nasal passage achieves greater airflow. The airflow through the each nasal cavity is then governed by the resistance caused by the cross-sectional area of each airway. Therefore this study investigates the time-dependent particle deposition during inhalation, using a negative gauge pressure at the nasopharynx which is caused by the lung expansion during the diaphragm movement. The unsteady particle deposition is then compared with an equivalent steady inhalation having a tidal volume of 500ml [13]. Two particle sizes, 5μm and 20μm are used to represent cases with contrasting Stokes numbers.

2. METHOD

2.1. Computational Model Construction

The nasal cavity geometry was obtained through a Computed Tomography (CT) scan of the nose of a healthy 25-year-old male Asian (175cm height and 75kg mass). The CT scan was performed using a CTI Whole Body Scanner (General Electric). The single-matrix scanner was used in helical mode with 1-mm collimation, a 40-cm field of view, 120kV peak and 200mA. The scans captured outlined slices in the X-Y plan at different positions along the Z-axis from the entrance of the nasal cavity to just anterior of the larynx at interval of 1mm to 5mm depending on the complexity of the anatomy. The coronal-sectioned scans were imported into a three-dimensional (3-D) pre-processing software called GAMBIT which created smooth curves by connecting points on the coronal sections. Due to the irregularity of the geometry, unstructured tetrahedrons were created for the mesh. The nasal cavity comprises of 3 regions – Anterior Region (nasal vestibules), Middle Region (olfactory turbinates) and Posterior Region (nasopharynx) as shown in Figure 1.

An initial model with 260,000 unstructured tetrahedral cells was refined until the skewness of the cells and Y_{plus} value on the walls dropped below 0.8 and 0.78 respectively. The final model consisted of 3.5 million cells which required the use of a HPxw6600 16Gb RAM, 8 processor workstation to perform the simulations. The computational model applied some assumptions to simplify the airway. The first assumption is that of rigid boundary walls. However this comes at the expense of the real physiological cyclic movement of the nasal passages. In reality, collapse of the nasal valve can occur at high breathing rates, leading to additional flow resistance. During normal breathing rates, the walls may also be subjected to stress/strain rates by the impinging airflow passing through, which in turn affects the flow field in a coupled approach. Implementing flexible walls requires knowledge of the material properties of the wall (such as its elasticity applied to a Fluid-Structure-Interaction model) which is quite difficult to perform while a person is actually breathing. The wall was also assumed to be smooth but it has been shown that the surface roughness due to presence of mucus and/or blocked areas in the presence of nasal hair can have an effect on the deposition [8, 15]. The second assumption is that nasal hairs were not considered in this paper. The influence of nasal hairs will have two effects on the inhalation of particles. Firstly the air flow field entering the nostril encounters a porous cross-section caused by the cilia, reducing the flow rate. The second effect is that particles are susceptible to deposition onto the cilia, especially for particles with larger diameters. This effect is primarily limited to the nasal vestibule (nostril and anterior nasal cavity region) where there is a high concentration of cilia. In addition it has been shown that the nasal hair influence is most significant for particles with diameters above 20μm and below 5nm [16].

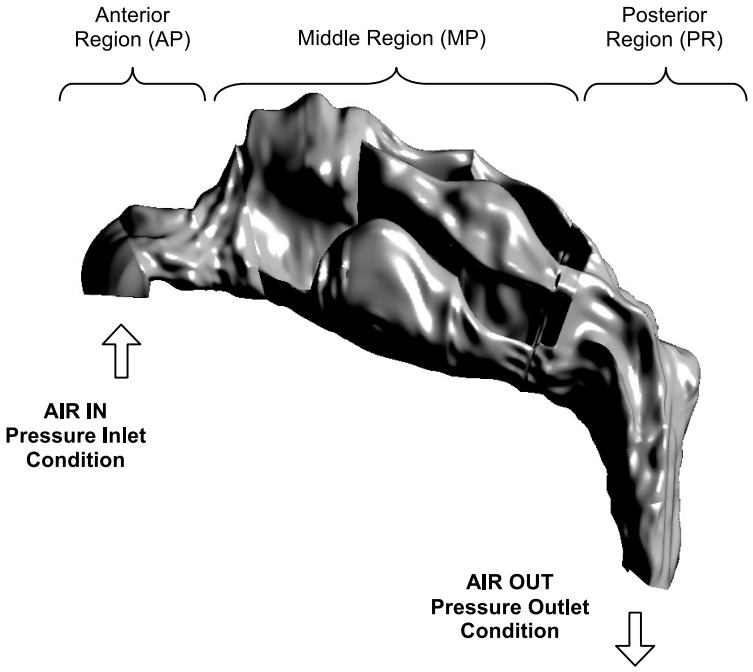

Figure 1. Schematic diagram of nasal cavity model. Thirteen coronal slices beginning at the nasal valve region through to the rear of the main nasal passage are created and labeled in the figure.

2.2. Numerical Modelling

Air movement through the nasal cavity is induced by the pressure difference initiated by the thoracic diaphragm at the bottom of ribcage. Thus, an unsteady negative pressure profile relative to the atmospheric pressure at nostril inlet is applied near the larynx to induce the inhalation. The inhalation profile was amended based on the inhalation profile measured from a healthy 50-year-old male volunteer (70kg weight, 170cm height) [13]. The inhalation profile has a maximum inhalation flow rate of 20L/min (corresponding to tidal volume of 500mL). The period of inhalation is set to 1.4s and the flow rate is adjusted in order to maintain the same tidal volume. The profile of the inhalation is presented in Figure 2 which has a maximum flow rate of 40.3L/min. For its equivalent steady flow rate, the inhalation cycle is time-averaged and is presented by a constant flow rate of 24.6L/min.

The CFD package ANSYS FLUENT was used to solve the unsteady incompressible fluid flow in the nasal cavity. The unsteady Reynolds-averaged mass continuity and momentum equations for the gas phase (air) are given in Eqn. (1) and (2) respectively.

$$\frac{\partial \rho}{\partial t} + \nabla \cdot \left(\rho \vec{U} \right) = 0 \tag{1}$$

$$\frac{\partial \rho \vec{U}}{\partial t} + \nabla \cdot \left(\rho \vec{U} \vec{U} \right) = -\nabla p + \nabla \cdot \left(\mu + \mu_t \right) + \left(\nabla \vec{U} + \left(\nabla \vec{U} \right)^T - \frac{2}{3} \delta_{ij} \nabla \cdot \vec{U} \right) + \rho g + \vec{F} \tag{2}$$

where $\mu_t = \rho \alpha^* \frac{k}{\omega}$; $\delta_{ij} = 1$ if $i = j$ and $\beta_{ij} = 0$ if $i \neq j$;

The QUICK scheme was employed to solve the momentum equation; while the SIMPLEC method was used to resolve pressure-velocity coupling. Although the Reynolds number at the nostril inlets at the peak inhalation rate of 40.3L/min is 2,250, the high degree of irregularity contributes to instabilities enhancing the transition to turbulent flow. Thus, the low-Reynolds Shear Stress Transport (SST) *k-ω* turbulent model was used to close the Reynolds averaged equations in Eqn. (1) and (2).

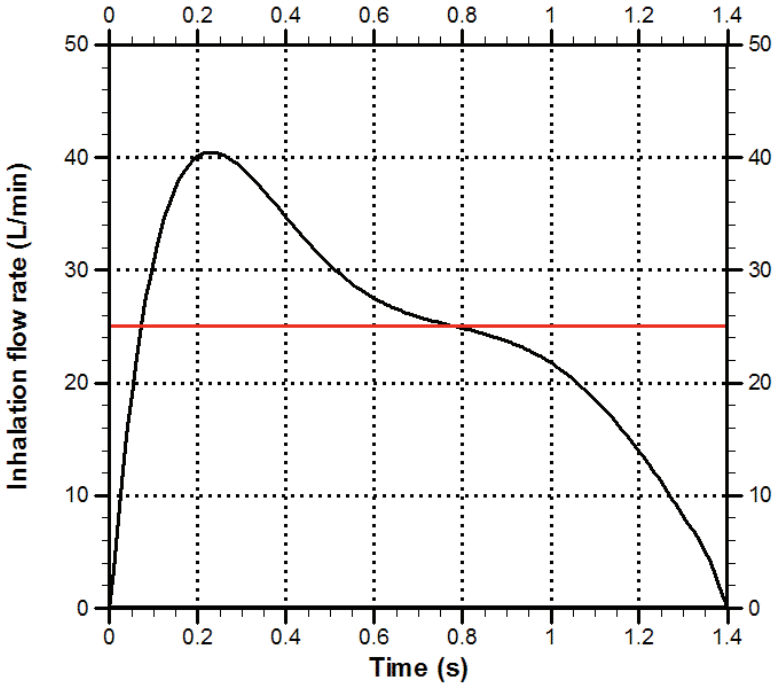

Figure 2. Pressure profile for the inhalation breathing cycle. The black line represents the unsteady inhalation cycle. The red line represents the equivalent steady inhalation.

The equations for turbulent kinetic energy, *k*, and the specific dissipation rate, *ω*, are given in Eqn. (3) and (4) respectively. A turbulence intensity of 5% is used, considering the external inhalation which may be affected by the facial features.

$$\frac{\partial}{\partial t}\left(\rho k\right)+\nabla\cdot\left(\rho\vec{U}k\right)=\nabla\cdot\left[\left(\mu+\frac{\mu_t}{\sigma_k}\right)\nabla k\right]+\tilde{G}_k-Y_k+S_k \tag{3}$$

$$\frac{\partial}{\partial t}\left(\rho\omega\right)+\nabla\cdot\left(\rho\vec{U}\omega\right)=\nabla\cdot\left[\left(\mu+\frac{\mu_t}{\sigma_\omega}\right)\nabla\omega\right]+\tilde{G}_\omega-Y_\omega+D_\omega+S_\omega \tag{4}$$

The particle trajectory was modelled by using a Lagrangian approach and integrating the force balance equations on each particle as follows.

$$\frac{du_p}{dt}=F_D(u_g-u_p)+\frac{g(\rho_p-\rho_g)}{\rho_p}+F_S \tag{5}$$

where

$$F_D = \frac{18\mu_g}{\rho_p d_p^2}\frac{C_D \mathrm{Re}_p}{24} \tag{6}$$

$$\mathrm{Re}_p = \frac{\rho_p d_p \left| u_p - u_g \right|}{\mu_g} \tag{7}$$

$$C_D = a_1 + \frac{a_2}{\mathrm{Re}_p} + \frac{a_3}{\mathrm{Re}_p^2} \tag{8}$$

in which *a*'s are the empirical constants for smooth spherical droplets over several ranges of droplet Reynolds number [17]. The second term in Eqn.(5) is the gravity term while the third term, F_s represents other possible forces such as virtual mass force, Basset force, pressure gradient force, lift force, thermophoretic force and Brownian force. The CFD code handles the turbulent dispersion of droplets by integrating the trajectory equations for individual droplets, using the instantaneous fluid velocity, $u_i^q + u_i'(t)$, along the droplet path during the integration process. Here, the Discrete Random Walk model (DRW) is used where the fluctuating velocity components u_i' that prevail during the lifetime of the turbulent eddy are sampled by assuming that they obey a Gaussian probability distribution. A near wall correction was applied to account for the anisotropic behaviour of turbulence by damping the turbulent kinetic energy as described in Matida *et al*. [18]. The function is given as,

$$k_{new} = [1 - \exp(-0.02y^+)]2\, k_{simulated} \qquad \text{for } y^+ < 30 \tag{9}$$

A total number of 10,000 particles were released passively at surfaces parallel to the nostrils and which was 5% smaller in diameter than the nostrils to avoid immediate particle deposition. A zero injection velocity was set to allow particles to move and deposit based on the induced pressure difference at each time step. All particles were released once at the initial time step of 0s so that the trajectory and residence times could be captured. Moreover, it is assumed that the particle will not affect the fluid flow (one-way coupling) as the volume fraction of the droplets was relatively low (<10%). Other assumptions include no particle rebounding off the walls/surfaces; no particle coagulation in the particle deposition process; and all particles are spherical and non-deforming.

2.3. Validation

Since experimental studies regarding the unsteady inhalation are limited in the literature, both pressure difference between nostrils and nasopharynx and the deposition efficiency for the present nasal cavity model were validated using steady inhalation. The averaged pressure differences at different inhalation flow rates [19-20] was compared with present model which were measured based on a constant inhalation rate. The steady inhalation at 24.6L/min and the peak inhalation rate of 40.3L/min from the unsteady inhalation gave an averaged pressure difference of 34.8Pa and 83Pa respectively. It was found that the present model is in excellent agreement with other studies (see Figure 3).

Monodispersed particles in the range of 1μm – 50μm were released passively into the nasal cavity model under flow rates of 5, 10, 15 and 20L/min. The deposition of particles as a function of the inertial parameter, ($d_a^2 Q$) is shown in Figure 4 which displays the characteristic curve associated with inertial deposition. Differences in deposition may be attributed to the inter-subject variability between the nasal cavity models (53 year-old Caucasian male) studied in Kelly *et al.* [19] with the model used in the present study (25 year-old Asian male). Besides, the nasal cavity replicate casts with wider airways can cause less deposition due to secondary flow [13].

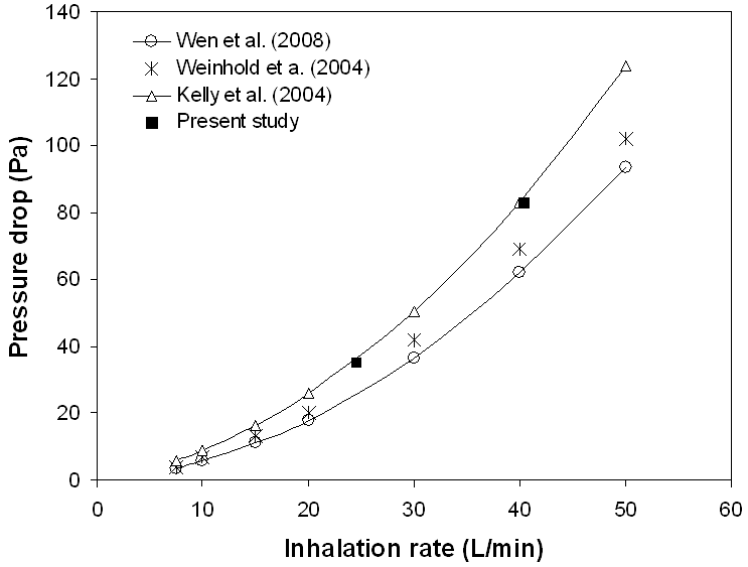

Figure 3. Pressure drop across the human nasal cavity as a function of inhalation flow rate compared with reported experimental works [19-20] and a numerical study [14]

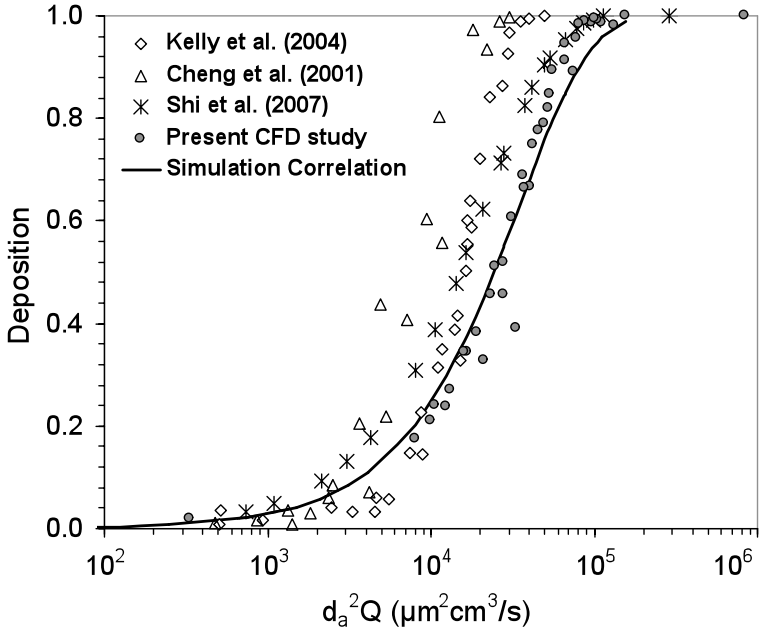

Figure 4. Total deposition of particles against inertial parameter compared with reported data [8, 19, 21]

3. RESULTS AND DISCUSSION

3.1. Particle Deposition

Quantitative analysis on the particle deposition is presented by deposition efficiency at different time steps. The efficiency versus time is presented in histogram or lines by the Escape efficiency (ESC), and the Absolute efficiency (ABS) defined as:

$$\text{ESC} = \text{particles escaped at } \Delta t \text{ / total particles released} \quad (10)$$

$$\text{ABS} = \text{particles deposited at } \Delta t \text{ / total particles released} \quad (11)$$

All transient results are presented at an interval of 0.1s. Any particles depositing during 0s to 0.1s will contribute to the deposition efficiency at 0.1s. Based on this method, the absolute deposition efficiencies versus time for 5μm and 20μm are shown in Figure 5 and Figure 6 respectively. It shows that the highest deposition for both particles was in the middle region (MR). Interestingly, higher deposition efficiency was found in posterior region (PR) in comparison with the anterior region (AR) for 20μm particle; while 5μm particle it is the other way round. The deposition of 5μm in AR was much higher than that in PR; while the 20μm gave a similar ABS in AR and PR.

Focusing on the ABS efficiency in the first 0.1s, the ABS for 5μm in the nasal cavity was only 4% while compared to the ABS efficiency of up to 55% in 20μm particles. Further analysis shows that the ESC efficiency of 5μm and 20μm particles is 69% and 20%, respectively (see Figure 7). Such significant difference in the ESC efficiency is caused by the particle inertia transport phenomenon. For large particles, inertia tends to dominate particle movement and reduces its dependence to the airflow (i.e. inertial deposition); while, smaller particles are more dependent on airflow structure (i.e. streamlines). Since the relaxation time of particle increases with particle sizes, local eddies do not impose as strong influence on larger particles as it does on small particle. As a result, stronger inhalation flow rate leads to higher ESC efficiency for small particles.

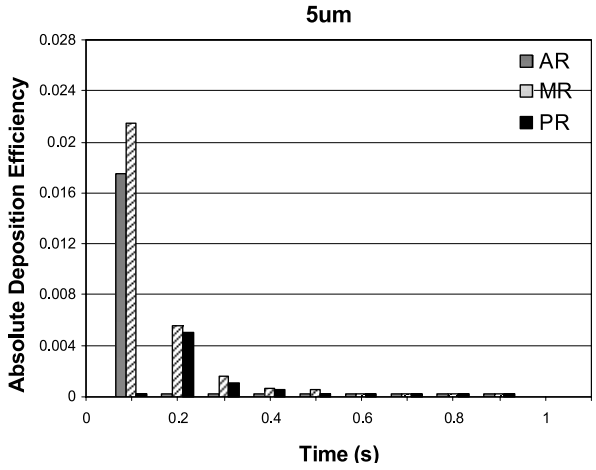

Figure 5. Absolute deposition efficiency of 5 m particle. AR = anterior region, MR = middle region, PR = posterior region.

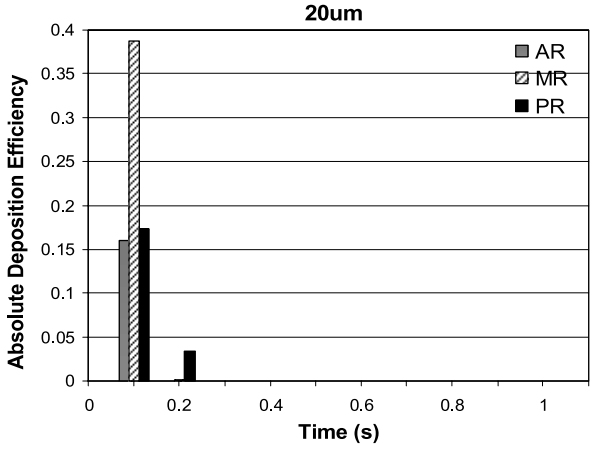

Figure 6. Absolute deposition efficiency of 20 m particle. AR = anterior region, MR = middle region, PR = posterior region.

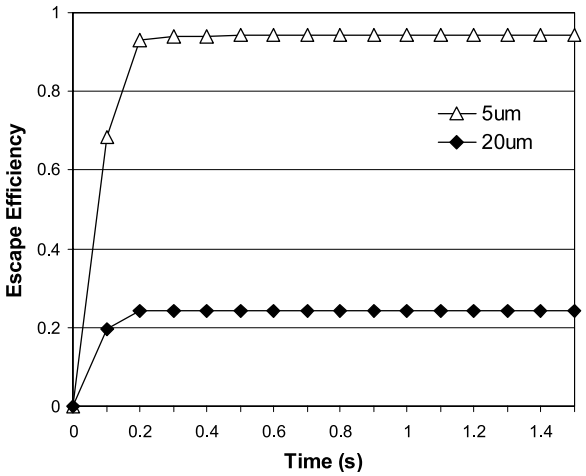

Figure 7. Escape efficiencies of 5 m and 20 m

As the inhalation further develops, more particles are deposited in the nasal cavity. It is noted that deposition of the 5μm particles occurs within the first 0.9s of the inhalation cycle while no further deposition of 20μm occurred after 0.2s. Therefore the rapid deposition of 20μm shows that large particle deposition does not have a strong correlation with the inhalation flow rate, but rather is more influenced by its diameter (as given by the Inertial Parameter, IP ∞d^2). Thus, in absence of further inhalation of particles, the transient deposition patterns of 5μm and 20μm are presented up to 0.9s and 0.2s respectively (refer Figure 8 and Figure 9).

These 2 particle sizes came to different deposition patterns along the nasal cavity, as well as the population of deposited particles. In general, 20μm particles deposited more densely in AR and MR than 5μm particles. Most of the 20μm particle was deposited on the inner walls of the MR while 5μm gave a more dispersed pattern over the entire nasal cavity. About 75% of 20μm particles were settled on the nasal cavity in 0.2s in comparing to 5% of 5μm particles at the same duration. Deposition of 5μm particles in the PR has a time lag of at least 0.1s where the deposition in the PR first begins at at 0.2s (see Figure 8b). In contrast, 20μm particles had already been transported to the nasopharynx bend at 0.1s (see Figure 9a).

In the presence of the nasopharynx bend in the airway, flow separation occurs and eventually, the 20μm particles deposit by inertial deposition. In the absence of further inhalation of particles, the first 0.2s is more crucial in deposition efficiency for 20μm under the unsteady inhalation profile. Although particle deposition finished at 0.9s, more than 90% of 5μm particles had already deposited or escaped down the nasopharynx towards the pharynx, at 0.2s. As a result, the ESC efficiency (see Figure 7) became constant after 0.2s, as no further particles were released.

3.2. Deposition under Steady versus Unsteady inhalations

The total deposition efficiencies between steady and unsteady inhalation are compared in this section. A steady flow rate of 24.6L/min is used, which has an equivalent tidal volume to the time-averaged unsteady inhalation cycle shown in Figure 2. The comparison between the deposition efficiencies obtained under steady and unsteady inhalation for 5μm and 20μm are presented in Figure 10 and Figure 11 respectively. Surprisingly, the deposition efficiencies of 5μm particle at steady and unsteady inhalation are very similar which give a total deposition of 8% for steady inhalation and 5.9% for unsteady inhalation. Among the regions, the unsteady inhalation produces less deposition in the range of 17%-50% for 5μm. The distribution of deposited 5μm particles along the nasal cavity is similar in both inhalation profiles where highest deposition is found in MR. For the 20μm particle, the total deposition efficiency is 97% and 75% under steady and unsteady inhalation respectively. However, the deposition efficiencies of 20μm particles for steady inhalation show different distribution among regions. Highest deposition is found in AR for steady inhalation; while the middle region is the highest for unsteady inhalation. Moreover, the deposition efficiency in the PR under steady inhalation is found to be triple of that with unsteady inhalation.

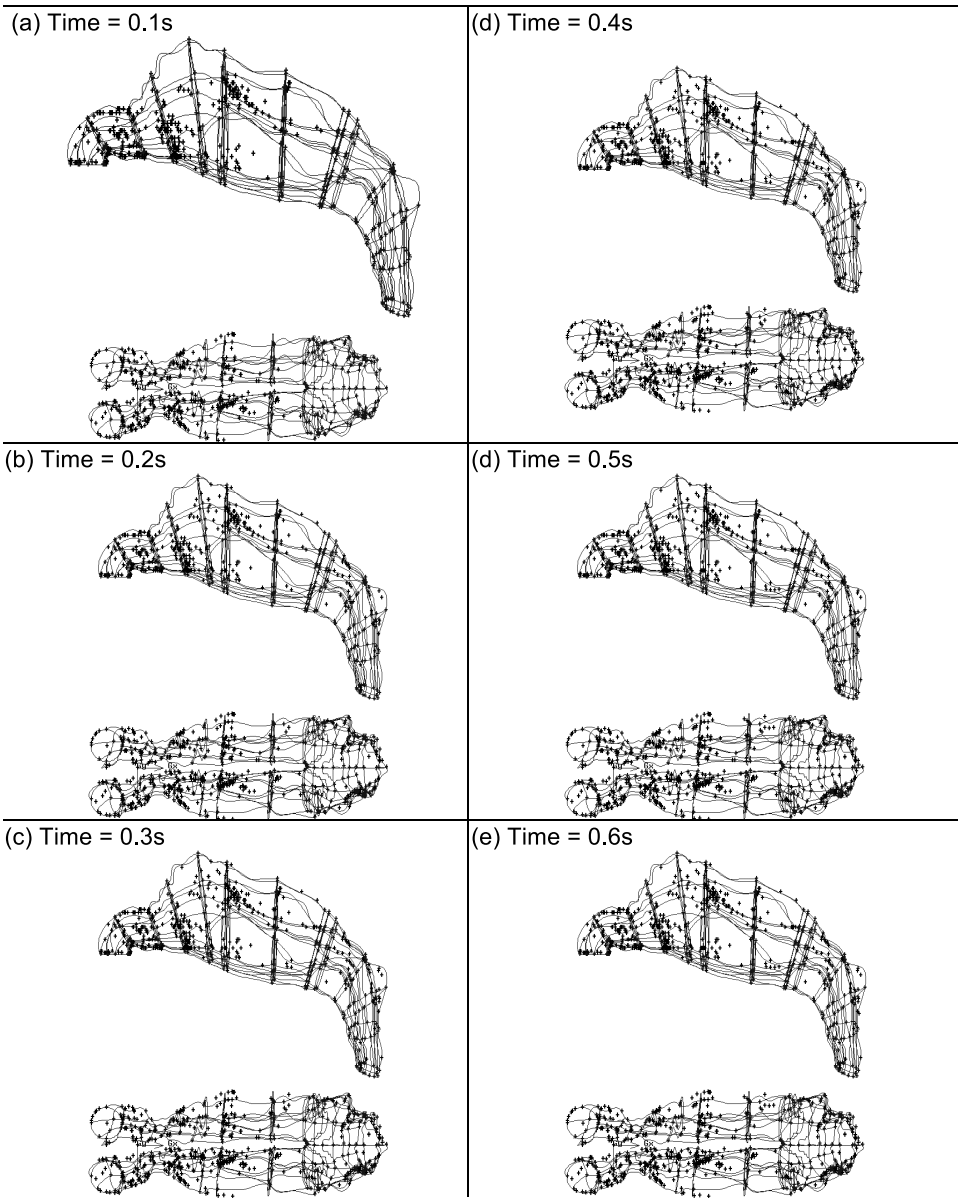

Figure 8. Unsteady deposition of 5 m particle at 0.1s interval

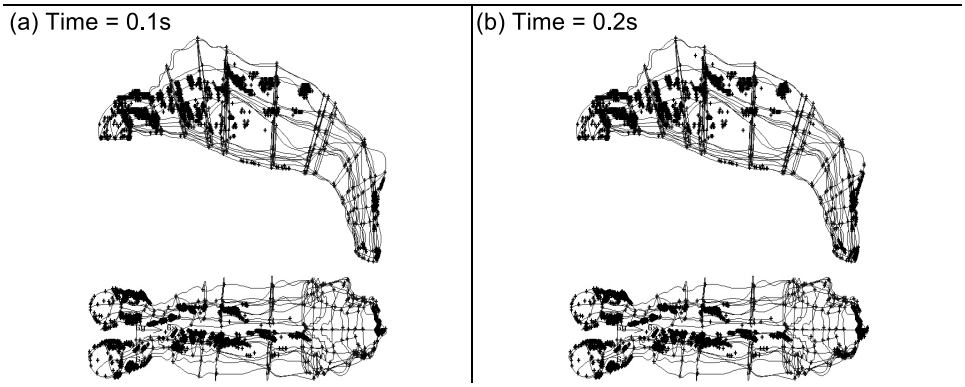

Figure 9. Unsteady deposition of 20μm particle at 0.1s interval

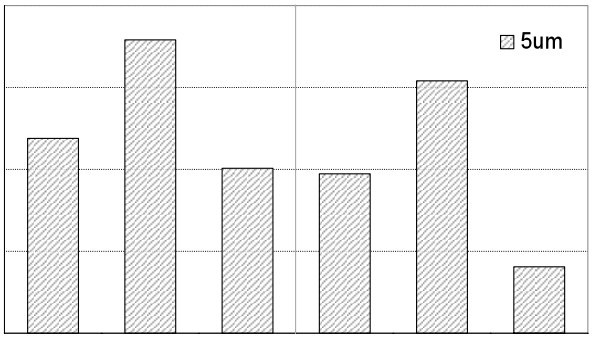

Figure 10. Deposition efficiency for 5 m

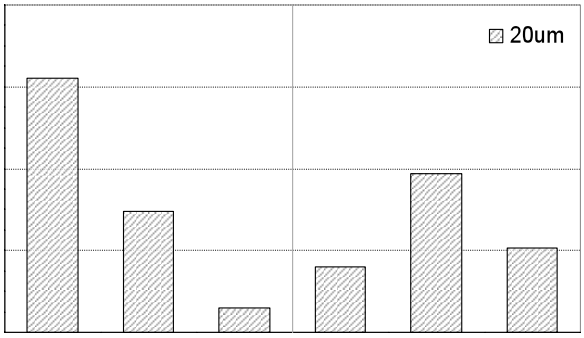

Figure 11. Deposition efficiency for 20 m

Based on the inertial particle transport phenomenon, the inhalation profile has a significant effect on the particle deposition efficiency. For a steady inhalation 94 % of 5µm particles escaped the nasal cavity domain, while only a slightly higher deposition resulted from the unsteady inhalation. However, for 20µm particles, the total deposition for unsteady inhalation decreased by about 25% for 20µm particles. This is because complete deposition of the 20µm particle occurs within the first 0.1s (i.e. residence time) of the inhalation cycle where within in this time step, a much slower mean airflow rate is present. After 0.2s the transport of the 20µm particle is completed, if not earlier. For the steady inhalation the 20µm particle experiences much higher flow rates immediately which is critical as the residence time in the nasal cavity is less than 0.2s. The steady inhalation result show that higher deposition in the AR (up to three times) occurs in comparison with unsteady inhalation. As a result the higher deposition in the AR, the deposition efficiency in the MR and PR are smaller.

A higher deposition for steady inhalation over unsteady was also found in the work conducted by Häußermann *et al.* [13], but this increase diminished as the particle size became larger. However, in the present study the effect of steady flow on higher deposition became greater as the particle size increased. In Häußermann *et al.* [13], the particle sizes studied were between 1 – 10µm which differs to the particle sizes used in this study. In addition, the topologies of the nasal cavity models are different. In contrast, Gurman *et al.* [22-23] studying deposition in the tracheobronchial tree, found that unsteady inhalation enhances deposition compared to steady inhalation. Based on the probability method introduced by Landahl [24], the deposition in the respiratory tract for an unsteady inhalation increased by about 15% for inertial deposition and decreased by 22% for sedimentation deposition over steady inhalation. Further investigation for other particle sizes may be performed in future to cover a wider range of particle size.

4. CONCLUSION

Time-dependent deposition efficiencies of 5μm and 20μm particles in a realistic nasal cavity were investigated by CFD techniques. An unsteady inhalation profile of a realistic breathing cycle measured by Häußermann *et al.* [13] with halve inhalation period was adopted. The modified unsteady inspiratory cycle has a peak inhalation rate of 40.3L/min. Particles were released passively at 0s. Two representations of deposition efficiency were presented to discuss the temporal deposition phenomenon. Based on the assumptions of smooth rigid walls and the absence of nasal cilia, the results for the deposition efficiencies in the anterior nasal cavity will be somewhat underpredicted. This becomes more significant as the particle diameter increases. Much higher total deposition efficiency was found with 20μm particles than that of 5μm particle. Based on the amended inhalation profile, single passive injection of two particle sizes came to different critical deposition times. All particles were deposited in the first 0.9s of the inspiratory cycle for 5μm particles; while 0.2s was required for 20μm particles. As the inhalation develops, escape efficiency was enhanced. The enhancement effect was more significant on low Stokes numbered particles than high Stokes numbered particles.

In comparison to the steady inhalation, unsteady inhalation led to lower deposition efficiency for 20μm particles while giving approximately the same deposition for 5μm particles. In the absence of further inhalation of particles, the regional deposition under steady and unsteady inhalations were similar for 5μm particles; while the allocation of large particle (i.e. 20μm) deposition altered because of the inertial-dominated transport characteristic. The deposition efficiency of large particles was exaggerated by 3 times due to a significant reduction in airflow velocity under steady inhalation. Since different findings were concluded among limited number of studies, further investigation on the effect of steadiness of inhalation on deposition efficiency in the future is needed.

REFERENCES

[1] Se, C.M.K., K. Inthavong, and J.Y. Tu, *Inhalability of Micron Particles through the Nose and Mouth.* Inhalation Toxicology, 2009. **22**(4): p. 287-300.

[2] Kennedy, N.J. and W.C. Hinds, *Inhalability of large solid particles.* Journal of Aerosol Science, 2002. **33**: p. 237-255.

[3] Anthony, T.R. and M.R. Flynn, *Computational fluid dynamics investigation of particle inhalability.* Aerosol Science, 2006. **37**(6): p. 750-765.

[4] Balashazy, I. and W. Hofmann, *Particle deposition in airway bifurcations—I. Inspiratory flow.* Journal of Aerosol Science, 1993. **24**(6): p. 745–772.

[5] Cheng, K.H., et al., *In-vivo measurements of nasal airway dimensions and ultrafine aerosol deposition in the human nasal and oral airways.* Journal of Aerosol Science, 1996. **27**(5): p. 785-801.

[6] Zhang, Z., C. Kleinstreuer, and C.S. Kim, *Comparison of analytical and CFD models with regard to micron particle deposition in a human 16-generation tracheobronchial airway model.* Journal of Aerosol Science, 2009. **40**(1): p. 16-28.

[7] Moskal, A. and L. Gradon, *Temporary and spatial deposition of aerosol particles in the upper human airway during breathing cycle.* Journal of Aerosol Science, 2002. **33**: p. 1525-1539.

[8] Shi, H.W., C. Kleinstreuer, and Z. Zhang, *Modeling of inertial particle transport and deposition in human nasal cavities with wall roughness.* Journal of Aerosol Science, 2007. **38**: p. 398-419.

[9] Inthavong, K., et al., *A numerical study of spray particle deposition in a human nasal cavity.* Aerosol Science Technology, 2006. **40**(11): p. 1034-1045.

[10] Zwartz, G.J. and R.A. Guilmette, *Effect of flow rate on particle deposition in a replica of a human nasal airway.* Inhal. Toxic., 2001. **13**(2): p. 109-127.

[11] Shanley, K.T., et al., *Numerical simulations investigating the regional and overall deposition efficiency of the human nasal cavity.* Inhalation Toxicology, 2008. **20**(12): p. 1093-1100.

[12] Subramaniam, R.P., et al., *Computational fluid dynamics simulations of inspiratory airflow in the human nose and nasopharynx.* Inhalation Toxicology, 1998. **10**(91-120).

[13] Häußermann, S., et al., *The influence of breathing patterns on particle deposition in a nasal replicate cast.* Journal of Aerosol Science, 2001. **33**(6): p. 923-933.

[14] Wen, J., et al., *Numerical simulations for detailed airflow dynamics in a human nasal cavity.* Respiratory Physiology & Neurobiology, 2008. **161**: p. 125-135.

[15] Katz, I.M., B.M. Davis, and T.B. Martonen, *A numerical study of particle motion within the human larynx and trachea.* Journal of Aerosol Science, 1999. **30**(2): p. 173-183.

[16] Swift, D.L. and J. Kesavanathan, *THE ANTERIOR HUMAN NASAL PASSAGE AS A FIBROUS FILTER FOR PARTICLES.* Chemical Engineering Communications, 1996. **151**(1): p. 65 - 78.

[17] Morsi, S.A. and A.J. Alexander, *An investigation of particle trajectories in two-phase flow systems.* Journal Fluid Mechanics, 1972. **55**(2): p. 193-208.

[18] Matida, E.A., et al., *Improved numerical simulation of aerosol deposition in an idealized mouth-throat.* Journal of Aerosol Science, 2004. **35**: p. 1-19.

[19] Kelly, J.T., et al., *Particle deposition in human nasal airway replicas manufactured by different methods. Part 1: Inertial regime particles.* Aerosol ScienceTech., 2004. **38**(11): p. 1063-1071.

[20] Weinhold, I. and G. Mlynski, *Numerical simulation of airflow in the human nose.* European Archive Otorhinolaryngology, 2004. **261**: p. 452-455.

[21] Cheng, Y.S., et al., *Characterization of nasal spray pumps and deposition pattern in a replica of the human nasal airway.* Journal of Aerosol Medicine, 2001. **14**(2): p. 267-280.

[22] Gurman, J.L., et al., *Particle deposition in replicate casts of the human upper tracheobronchial tree under constant and cycle inspiratory flow I: Experimental.* Aerosol Science and Technology, 1984. **3**(3): p. 245-252.

[23] Gurman, J.L., et al., *Particle deposition in replicate casts of the human upper tracheobronchial tree under constant and cycle inspiratory flow II: Empirical model.* Aerosol Science and Technology, 1984. **3**(3): p. 253-257.

[24] Landahl, H., *On the removal of airborne droplets by the human respiratory tract: I. The lung.* Bulletin of Mathematical Biophysics, 1950. **12**: p. 43-56.